CrystEngComm

Accepted Manuscript

Journal Name

CrystEngComm

Dynamic Article Links ►

Cite this: DOI: 10.1039/c0xx00000x

www.rsc.org/xxxxxx

ARTICLE TYPE

X-ray Irradiation Induced Reduction and Nanoclustering of Lead in a Borosilicate Glass

Halina B. Stanley[a], Dipanjan Banerjee[a], Lambert van Breemen[e], Jim Ciston[b], Christian H. Liebscher[b], Vladimir Martis[a], Daniel Hermida Merino[a], Alessandro Longo[a], Philip Pattison[c], Gerrit W.M. Peters[e], Giuseppe Portale[a], Sabyasachi Sen[d] and Wim Bras[a]

Received (in XXX, XXX) Xth XXXXXXXXX 20XX, Accepted Xth XXXXXXXXX 20XX
DOI: 10.1039/b000000x

We have studied the formation of nanoparticles in a lead sulfide (PbS) doped borosilicate glass subjected to a two-step nucleation and growth heat treatment, using in-situ small angle X-ray scattering (SAXS). The microstructure produced was subsequently characterized using X-ray powder diffraction (XRD) and transmission electron microscopy (TEM). While PbS nanocrystals of diameter ca. 2 nm are formed throughout the sample during the heat treatment, larger monodisperse Pb nanocrystals (diameter ca. 50nm) are formed due to exposure to the X-ray beam, yielding space selective nanoparticle growth. The time-resolved SAXS spectra are in the early stages consistent with diffusion limited growth of the Pb particles. We attribute the X-ray induced formation of nanocrystalline Pb to X-ray photo reduction of the Pb^{2+} atoms.

Introduction

X-ray diffraction is generally regarded by the materials science community as a non-destructive characterization technique that is able to probe microstructure of solids in-situ. However, in spite of being generally viewed as benign compared to electron microscopy or laser irradiation, intense synchrotron X-ray beams can lead to radiation damage,[1-3], or even to structure formation[4-6]. Despite a significant body of knowledge about radiation damage in soft condensed matter[7], aqueous[8, 9] and biological systems[10-14], little has been reported about the structure modifying interactions of monochromatic photons in the $5 < E < 40$ keV range in hard condensed matter such as crystalline or vitreous materials. In such samples radiation damage has usually been considered to be negligible since the energy levels are too low for direct atomic displacements [15]. Sample heating due to absorbed X-rays is not thought to play an appreciable role either, unless one is working on samples close to the absolute zero temperature or using white beam techniques[16]. Nevertheless, the possibility of X-ray induced electron transfer and corresponding oxidation-reduction processes cannot be neglected.

Controlled precipitation of metallic and semiconductor nanoparticles in glass is of interest to photochromic glass and glass ceramics technology[17] as well as in the areas of photonics, optoelectronics and catalysis[18-23]. Semiconductor nanocrystals or quantum dots (QDs) of Pb based IV-VI semiconductors (e.g. PbS, PbSe, PbTe) are particularly interesting as they show some of the strongest quantum confinement effects, owing to their relatively large exciton Bohr radii[24]. This attribute makes the Pb-based IV-VI quantum dots particularly attractive materials for applications in nonlinear photonics and solar cells. One of the simplest preparation routes for producing quantum dots embedded in an inert and durable matrix still remains solid-phase precipitation of QDs in glassy hosts via nucleation and growth[18, 25]. Synthesis of QDs by nucleation and growth in glasses is particularly attractive as it is an inexpensive and relatively easy way to form quantum dots with excellent size control[26].

Owing to the high electron density contrast between PbS particles and oxide glasses, such characterization is ideally suited for time-resolved Small and Wide Angle X-ray Scattering (SAXS/WAXS) [27, 28]. Here we report the results of an in-situ small-angle X-ray scattering study of the thermally induced nucleation and growth of PbS quantum dots in a borosilicate host glass and the serendipitous finding that larger Pb crystals form under the influence of the X-ray beam. This result suggests that deep X-ray lithography, which has been used to create functional materials by direct patterning of sol-gel, hybrid organic-inorganic and mesoporous films[29], could also be applied to borosilicate glasses at elevated temperatures.

Experimental

Glass Synthesis

A borosilicate glass of composition (mol%) 58.7% SiO_2-21.4% K_2O-7.1% B_2O_3-3.0% CaO- 8.8% BaO, nominally doped with 2 wt% PbS, was prepared by melting from constituent oxides (and carbonates for K and Ca) and PbS, in a silica crucible for 4 hours at 1400 ˚C in air. The melt was homogenized by mechanical stirring and cast on graphite. The resulting glass was annealed at 500 ˚C for 30 minutes before cooling down to ambient temperature by shutting off the furnace. The loss of S from the melt via sublimation and of Pb via high temperature reduction followed by density separation results in glasses that contained approximately 0.8 mol% Pb and 0.06 mol% S, as determined by electron probe micro-analysis (EPMA). The local environment of the lead atoms was verified using fluorescence EXAFS and transmission EXAFS using the BM26A beam line at the ESRF[30] at 80K in an Oxford Instruments cryostat. The Pb L_{III} edge (13.035 keV) EXAFS spectra obtained on the glass samples before heat treatment show most lead atoms have oxygen nearest neighbours and could be fitted without introducing Pb-Pb or Pb-S interactions, indicating that neither metallic Pb particles nor PbS (galena) form during the initial sample preparation.

Small angle X-ray scattering (SAXS)

Samples of dimensions 3mm × 5mm × 50µm were prepared for SAXS measurements which were carried out on beam line BM26B[31] at the European Synchrotron Radiation Facility in Grenoble and on beam line 7.3.3 at the Advanced Light Source (Berkeley) [32].

All samples underwent a 2-step heat treatment consisting of a particle nucleation anneal at 575 °C followed by an isothermal particle growth anneal at a higher temperature. Two experimental protocols were followed for the lower temperature anneal used to nucleate PbS quantum dots.

One series of samples was annealed in a tube furnace in air at 575 ºC for 6 hours (*ex-situ* nucleation); the samples reached 575 ºC from ambient within 20 minutes with negligible temperature overshoot. These pre-nucleated samples were then measured in-situ in the X-ray beam whilst undergoing an isothermal anneal at 630 ºC, 640 ºC or 650 ºC in a thermal gradient free furnace for up to five hours.

The second set of samples was annealed in a furnace at 575 ºC for 2 to 3 hours in the presence of X-ray beam (*in-situ* nucleation) immediately followed by an isothermal in-situ particle growth anneal identical to that described above.

SAXS data were collected continuously at a photon energy of 12 keV at a rate of one frame (data set) per minute using a Dectris Pilatus 1M area detector[33]. The X-ray flux was 5×10^{11} photons/s on a 300µm diameter spot. The scattering vector is given by $q = 4\pi sin\theta\lambda^{-1}$

The area directly irradiated during the SAXS experiments is significantly smaller than the total sample size, so irradiated and non-irradiated parts with identical thermal history could subsequently be characterized by X-ray powder diffraction and electron microscopy. These areas are hereafter referred to as "irradiated" and "non-irradiated". By virtue of the in-situ measurements, all SAXS data correspond to "irradiated" areas. SAXS patterns were corrected for incident X-ray intensity, sample transmission and background scattering using the FIT2D software package[34]. The software package SASfit[35] was used to model these SAXS patterns.

X-ray powder diffraction (XRD)

XRD data were collected from samples previously heat treated and measured in the SAXS experiments using a spot size of 0.5 mm^2 aligned on areas darkened (irradiated during the SAXS measurement) and immediately adjacent (non-irradiated) using the Swiss-Norwegian BM01A beam line at the ESRF, Grenoble. Samples were mounted between 25µm thick kapton support sheets and were rotated back and forth through 10˚ in the X-ray beam in order to minimise the measurement of incorrect peak intensities which can arise if the crystallites are not randomly oriented in the sample. Data were collected using a Dectris Pilatus 2M area detector[36] at an incident energy of 17.8 keV.

TEM

Scanning Transmission Electron Microscopy (STEM) data were collected on the aberration-corrected TEAM 0.5 instrument at the National Center for Electron Microscopy at Lawrence Berkeley National Laboratory. Samples were prepared by the Focused Ion Beam liftout technique[37] from both X-ray irradiated and non-irradiated regions of the sample. The resulting samples were thinned to approximately 100 nm in order to reduce the effects of damage from the Ga^+ ion beam. STEM data was collected in high-angle annular dark field (HAADF) mode at 300 kV with a convergence angle of 19 mrad and a collection angle of 68-340 mrad. Using custom software written in Matlab®, a total number of 950 particles were automatically detected from a series of STEM images of the X-ray irradiated region. The images were smoothed by a Gaussian filter before particle detection. The particle detection was performed on gradient images to treat regions with different background levels and hence different thicknesses simultaneously. Rough particle locations were determined by thresholding of the gradient image. Particle centers and radii were then obtained by a circular Hough transform as implemented in Matlab® with highest possible sensitivity to detect small features of less than 10 pixels and to account for agglomerated particles.

Results

SAXS

The SAXS patterns obtained after X-ray irradiation at 575 °C for 2.5 hours in-situ show no measureable difference to those obtained after ex-situ anneal at 575 °C for 6 hours. These SAXS patterns are consistent with the presence of particles of diameter ca. 2nm. When the temperature is raised to 630 °C or higher, rapid particle growth commences with particles of the order of 14nm diameter formed after 30 minutes. Figure 1 illustrates the evolution over a five hour isothermal anneal at 640˚C, where zero minutes corresponds to the pattern obtained at the end of the 575°C pre-anneal. Surprisingly, a simple sphere model for the particles, whether monodisperse or of a simple polydisperse form such as log-normal, is unable to reproduce the higher q (> ≈ 0.6 nm^{-1}) scattering intensity as the anneal progresses. These data imply the persistent presence of a significant population of small (radius ≈ 1-2 nm) particles in the samples, but are too background sensitive to permit detailed analysis of this particle size distribution. Using data containing clear structure a model consisting of a bimodal log-normal distribution of spherical particles was found as illustrated in Figure 2. These fit parameters were then extended interatively to shorter and longer times. Polydispersity increases at long anneal times which may be interpreted by growth of the smaller particles (also suggested by TEM) or Ostwald ripening of the larger particles (or both). The temporal evolution of the radius of the larger particles is shown in Figure 3. The mean particle radius R initially grows with time t as $R(t)\sim t^{1/2}$ but slows down at longer times $R(t)\sim t^{1/3}$. This is consistent with a crossover from diffusion limited growth at short times to Ostwald ripening at long times[38].

Pb L_{III}-edge EXAFS

The formation of PbS nanocrystals upon heat treatment is manifested in the appearance of Pb-S nearest neighbors and Pb-Pb next-nearest neighbors in the EXAFS spectra. No significant differences are observed between samples nucleated in-situ and ex-situ. The X-ray beam size is larger than that employed for SAXS measurements so it is not possible to select solely an irradiated area; both irradiated and non-irradiated areas of the sample were measured simultaneously.

Powder diffraction

The XRD pattern obtained from the glass sample after irradiation during the SAXS measurements, and specifically from the directly irradiated area, is shown in Figure 4. The pattern shows both very broad diffraction peaks corresponding to small crystallites of PbS and much sharper peaks arising from considerably larger particles of crystalline material. Close inspection reveals that there must be at least two of these crystalline phases in addition to PbS, since these data include peaks with a width limited by the instrumental resolution, together with peaks that are slightly broadened. The broadened reflections correspond to metallic lead. Analysis of the Scherrer broadening of these peaks gives diameters for the particles of PbS: 2(1) nm and Pb: 57.7(8.3) nm for one sample and PbS: 2(1) nm, Pb: 36.6(1.6) nm for a second. We therefore conclude that the evolving scattering pattern in the SAXS data during high temperature anneal corresponds to the growth of nanoparticles of metallic Pb.

In contrast, regions of the samples not exposed to X-rays during the SAXS measurements (non-irradiated regions) show no evidence for the presence of elemental Pb nanoparticles. This is illustrated in Figure 5 where the difference in scattering obtained between irradiated and non-irradiated positions of the same sample shows that the components are identical except for the presence of Pb.

Analysis of XRD patterns taken from the irradiated areas after the *in situ* SAXS anneal yields the relative ratios of 3.84(0.26)% Pb:96.16(0.26)% PbS from one sample and 6.63(0.28)% Pb:93.37(0.28)% PbS from a second. This ratio is remarkably different, and approximately reversed, from the ratio of Pb: PbS of ~ 93%:7% obtained from chemical analysis of the original glass, which EPMA gave as 0.838(0.057) mol % Pb and 0.059(0.012) mol% S. Since the XRD analysis is only sensitive to crystalline material, this observation indicates that most of the lead remains dispersed through the matrix, coordinated with oxygen, in agreement with the Pb L_{III}-edge EXAFS results.

The identity of the phase or phases producing the remaining narrow diffraction peaks is not clear at this stage. These peaks change dramatically in intensity and even presence over the sample surface. This suggests large crystals with preferred orientation, such as might be formed at the surface. SEM images (which we include as supplementary information) show just such crystals. Although of academic interest, these surface crystals are very unlikely to be of relevance to the bulk effects we describe.

Optical Microscopy

The changes in morphology inferred from the SAXS and XRD data are also evident in the macroscopic sample appearance. After annealing the samples are optically darkened in the region illuminated by the X-ray beam, the remainder of the sample merely gaining an inhomogeneous yellowish-brown tint.

TEM

The TEM images of the irradiated region of a sample annealed for 5 hours at 640°C clearly show two well-defined populations of spherical particles agreeing with the SAXS and XRD results discussed above (see Figure 6). The larger particles have a diameter of 54 ± 6 nm; the smaller particles are more polydisperse with an average diameter of 18 ± 5 nm with a size range of 10 to 30 nm in diameter (see Figure 7). There is no evidence from the HAADF STEM images that the larger Pb particles are a core-shell mixture of Pb and PbS.

A region of the same sample, imaged just outside the irradiated area, is illustrated in Figure 8. In this area the PbS particles are smaller, and close to the 2-3nm range observed by SAXS and XRD. The large particles are entirely absent in this area, again agreeing with the XRD data.

Discussion

Photo reduction of Pb

Visible and ultraviolet light are known to cause photo induced modifications in certain glasses including silver containing glasses and chalcogenide glasses[15]. The conventional wisdom is that the incident photons excite electrons leading to anisotropic charge distributions and bond breakage. Both photo-induced precipitation of silver metal out of a silver chalcogenide glass [39] and diffusion of silver ions into the irradiated region of a silver chalcogenide glass[40] have been observed in this way. X-ray photons have higher energy, but even the most intense X-ray beam produces several orders of magnitude fewer photons than for instance the 500W mercury lamp used in the cited manuscripts. Nevertheless X-ray irradiation also alters nanoparticle formation in glasses. In-situ X-ray irradiation of a soda-lime glass has been shown to assist the formation of gold nanoparticles, increasing the number of particles by an order of magnitude and delaying Ostwald ripening[5]. These authors hypothesise that defects serving as nucleation sites are created by the X-ray irradiation despite the elevated temperature of the in-situ anneal. It has also been reported that irradiation by 10keV X-rays from a synchrotron source not only increases the number of crystallisation nucleation sites in the region directly exposed to the beam, but also far beyond; an effect ascribed to photo electrons created by scattered radiation[4].

In addition there is a growing body of evidence that X-ray irradiation reduces metallic cations in glasses. Nanosized gold particles have been produced by reduction of Au^+ under Rh Kα irradiation at 600 °C[41] where we note simultaneous irradiation and heating was necessary. Reibstein et.al. observe the reduction of Ag^+ to Ag^0 under Cu Kα radiation in ionic sulfophosphate glasses[42], Eichelbaum et.al. describe the synchrotron X-ray radiation induced reduction of Au^+ to Au^0 and of Ag^+ to Ag^0 in soda lime silicate glasses[43], Ferreira et.al.[44, 45] and Zhang and Sheng[45] observe the synchrotron X-ray photo reduction of Fe^{3+} in low iron content soda-lime silicate glasses, whilst Vahedi et.al.[46] describe the synchrotron X-ray reduction of Sm^{3+} to Sm^{2+} in fluorophosphate and fluoroaluminate glasses. Finally Corrias[47] has evidence for the reduction of Cd^{2+} during X-ray Cu Kα irradiation of a glass system containing CdSe dots surrounded by CdS arms ("octopods") at room temperature. Ferreira et.al.[44] note that a fairly constant amount of iron was photo reduced by the synchrotron beam, whatever the total iron content in the sample. These authors also found that the photo reduction could be prevented by increasing the temperature.

In the present work we report that simultaneous X-ray irradiation and high temperature promotes the formation of metallic nanoparticulate Pb. Such particles cannot be formed in the glass by thermal annealing without irradiation and X-ray promoted growth of Pb nanoparticles has not previously been reported to the best of our knowledge.

Pb exists in considerable excess over S in the as-prepared glass. However, Pb L_{III}-edge EXAFS results indicate that practically all Pb in the as-prepared glass is in an oxide-like environment. Annealing at a temperature of 640 ºC allows breaking of Pb-O bonds and thermal diffusion of the resulting Pb^{2+} through the glass to combine with S to form clusters of PbS, irrespective of irradiation. Our sample preparation protocol appears to produce a great many nucleation sites leading to a large number of small galena particles and a rapid exhaustion of sulfur. The thermally driven formation of PbS particles is no surprise. In contrast, the formation of pure Pb crystallites in the irradiated volume is unexpected. Lead can exist as either Pb^{4+}, when incorporated as a networkformer in the glass network, or as Pb^{2+} when this is not the case. Evidently, even if the Pb atoms are capable of thermally driven diffusion through the network, crystallite formation is not possible unless the charges are somehow compensated. We observe a fairly monodisperse population of relatively large particles of Pb in X-ray irradiated regions, suggesting a small number of nucleation sites for their growth.

The question then arises as to whether the X-ray radiation provides photoelectrons for the reduction of Pb^{2+} to form Pb^0 atoms. It is known that X-ray irradiation may induce various defects such as nonbridging oxygen hole centers (NBOHC), boron oxygen hole centers (BOHC), boron electron centers and even alkali electron centers (where alkali cations trap electrons) in borosilicate glasses[41, 48, 49]. These electronic defects are unstable; they may be annealed out by raising the temperature to a few hundred degrees, or they decay over months or years at room temperature. Several authors suggest that NBOHC or BOHC provides electrons that can combine with neighboring cations to reduce the latter[41, 44, 46]; increasing the temperature allows these defects to relax and inhibits the photo reduction process. In our system we suggest that lead cations trap electrons under X-ray irradiation

$$Glass \xrightarrow{X-rays} D^+ + e^-$$

$$Pb^{2+} + 2e^- \rightarrow Pb^0$$

where D^+ is a defect. The D^+ defects may subsequently relax via local bonding reconstructions at these elevated temperatures. For example, if D^+ represents defects associated with excess oxygen such as NBOHC then the latter may be annealed by evolution of the excess oxygen from the glass. Once formed, the Pb^0 atoms, despite their larger radius, are expected to be significantly more mobile than Pb^{2+} ions, as the former do not bond with other atoms. These Pb^0 atoms diffuse through the glass structure and combine with other Pb^0 atoms to form nanoclusters of Pb metal that subsequently grow with time. It may be noted here that only a small fraction of nanocrystalline Pb compared to PbS is formed; the limiting factor is not the amount of Pb in excess of S in the glass. The limiting factor is most probably the defect concentration required for the generation of photoelectrons responsible for the reduction Pb^{2+} ions.

X-ray heating

Creation of particles of lead of up to 50nm diameter obviously implies diffusion within the glass and relaxation of the network. Whilst a temperature of 640 ˚C might be considered to be thermodynamically sufficient, the observation that these particles are only formed in the irradiated area of the sample leads us to consider whether beam heating effects may play a role. Beam heating is an important consideration for samples irradiated by X-ray free electron laser (XFEL) sources[50, 51] but, although individual photons in these beams may carry similar energies to synchrotron X-rays, fluxes are so high in XFEL sources that the energy deposited in samples is of the order of 10^{16} - 10^{17} Wcm^{-2}. In this study we have a flux of ~$5x10^{11}$ photons/s at an energy of 12 keV on a 300 µm diameter spot. This translates to a power of 1.36 Wcm^{-2}, which is very small compared to any kind of laser irradiation. Beam heating effects are sometimes observed at these fluxes in low temperature X-ray diffraction studies where the heat capacity and thermal conductivity become very small[52], but they are usually negligible in inorganic samples at room temperature. Typically thermal diffusion results in efficient thermal spreading of the deposited energy and almost uniform internal temperatures (see [16] for example) but structural changes attributed to X-ray beam heating by similar fluxes have been reported[53, 54].

Macroscopic heating is surely negligible (as commented above), but the question of differential heating of the heavily absorbing clusters of lead (and perhaps consequently their nanoscale environment) on a very local, and transient, level remains. We have therefore modeled the transient heating expected for lead particles dispersed in the glassy matrix due to radiation absorption. We consider one particle with a spherical shape, radius R_0 and temperature T(t). The problem is formulated in spherical coordinates such that the temperature equation reads:

$$\frac{dT}{dt} = \frac{\lambda}{\rho \cdot C_p}\left(\frac{\partial^2 T}{\partial r^2} + \frac{2}{r}\frac{\partial T}{\partial r}\right) + \frac{i}{C_p \cdot m_p}$$

in which λ [J/m.K.s] is the heat conduction coefficient, ρ [kg/m^3] is the density, C_p [J/kg.K] the heat capacity at constant pressure, i [J/s] the photon energy absorbed by the nano particle (estimated from the incident photon flux and the absorption coefficient of lead[55]) and m_p is the mass of the nanoparticle. Every particle is surrounded by a volume of the matrix material with radius R_1 that is half of the average distance between the dispersed particles. At this distance the heat flow is assumed to be zero. We do not consider any boundary effects around the particle, nor do we consider the macroscopic heat sink. The initial and boundary conditions are thus given by:

$$T(r, t = 0) = 0; \qquad T(0, t) = T_p; \qquad \nabla_r\big(T(r = R_1, t)\big) = 0$$

The absorption in the matrix material is assumed to be zero. This transient temperature problem is solved numerically using MATHEMATICA, applying the numerical method of lines[56]. For a lead particle with radius R_0=1 nm, $i = 8.526 \times 10^{-18}$ [J/s] and the material parameters given in Table 1 we obtain the transient temperature profile illustrated in Figure 9.

Table 1 Material Parameters

	Particles	Matrix
ρ [kg/m^3]	11340	2200
c_p [J/kg.K]	128.62	750-830
λ [J/m.K.s]	35.3	1.08-1.2

Over a time scale of 10^{-10}s the particle warms by some 4x10^{-11}K. If the simulation is allowed to continue for 10s the particle warms by 0.5K with negligible temperature gradient between particles; this situation would be counteracted in reality by a decrease in external heating power, leading us to the conclusion that beam heating effects are non-existent in accordance with the very low power absorbed.

Nevertheless, although the time averaged energy absorbed is very small, it is important to remember that the photon energy arrives in quanta. Using the linear absorption coefficient of lead we calculate that one photon is absorbed by a r=1nm spherical nanoparticle every 3¾ *minutes* on average in our experimental configuration; averaging over a second is very misleading. If the energy of one 12keV photon absorbed by an r=1nm radius nanoparticle of lead were converted adiabatically to heat this would correspond to increasing the temperature of the nanoparticle by 3.15x10^5 K! This simplistic classical view is wrong; photon energy is absorbed and then re-radiated by the absorbing atom via several processes over a distance related to the energy absorption cross-section[55]. What energy will ultimately be dissipated as heat (and where) depends on details of the electron-phonon coupling and is beyond the scope of this paper, however, a lower bound on the effect can be found by using the bulk energy absorption coefficient of lead[55]. This value leads to 0.014% of the photon energy being retained (and ultimately converted to heat) within a linear distance of 1nm. This is equivalent to a temperature increase of 44K, and since these processes occur on attosecond and femtosecond time scales would be an adiabatic effect. Numbers are arguably higher if the real geometry is considered. Glass is a much weaker photon absorber, and the linear energy absorption coefficient is a factor of 40 lower, so energy deposition is concentrated in the lead rich regions. Thus in our system, where the Pb diffusion coefficient depends strongly on temperature, heating cannot be excluded over distances of a few nm and time scales of 10^{-10}s to 10^{-9}s. This may also explain the increased size and definition of the PbS particles in the irradiated compared to the un-irradiated portion of the sample measured by TEM.

Kinetics of growth of Pb nanocrystals

The kinetics of crystallization of the Pb nanoparticles can be analyzed using the Avrami equation[57] where the volume fraction of the crystallized phase $\alpha(t)$ is given by

$$\alpha(t) = 1 - \exp[-Kt^n]$$

The constant K depends on details of the crystallites' growth rate and shape, and n, the "Avrami exponent", has a theoretical value between 1 and 4 determined by the dimensionality of growth and whether growth is interface or diffusion limited. The TEM images show that we have grown spherical particles to a good approximation. For monodisperse particles the crystalline volume fraction is therefore proportional to the particle radius R^3 and R can be determined directly from the SAXS data. For 3-dimensional growth, the Avrami exponent, n, may be described by

$$n = \not{k} + 3m$$

Where the number of particles $N \sim t^{\not{k}}$ and the size of the crystallite $\sim t^m$. For nucleation *followed* by growth (zero nucleation rate) $\not{k}$=0 ; for interface limited growth m=1; diffusion limited growth m = ½ [58] .

The variation in the size of Pb nanoparticles, as determined by SAXS, follows the Avrami function to a good approximation and yields an Avrami exponent of 1.8 (±0.5); consistent with a fixed number of particles (zero nucleation rate) and diffusion limited growth. This result is also qualitatively consistent with the observation that at the early stages we have a rather monodisperse distribution of particle sizes over a long anneal time

Figure 3 shows that there is not an unlimited growth of the particles. After the initial growth, which the SAXS data show render a rather monodisperse Pb particle population, the growth rate slows down. This is accompanied by a broadening of the particle size distribution: the SAXS patterns show a slow drift of the form factor fringes to lower q-values, i.e. particle growth, but accompanied by the scattering fringes becoming less pronounced, i.e. an apparent increase in polydispersity. This behaviour is consistent with an Ostwald ripening process in which the larger particles grow at the expense of smaller ones and $r(t) \propto t^{1/3}$ (see Figure 3). Since we do not observe an increase in scattering intensity we can rule out further additions of Pb from the matrix. This does not necessarily indicate that the matrix is depleted in Pb^{2+}, rather, it indicates that the matrix is depleted in Pb^0. We suggest that the concentration of Pb^0 is determined by the number of Pb^{2+} interactions with X-ray photo electrons and the life time of these Pb^0 atoms, The number, the life time and the diffusion rate determine if these atoms are available for further increasing the size of the Pb particles and it is not surprising that an equilibrium between the Pb in the matrix and the Pb in particles is established.

Conclusions

In the present work we report that X-ray irradiation at elevated temperatures promotes the formation of metallic nanoparticulate Pb. Such particles cannot be formed in the glass by thermal annealing without irradiation and X-ray promoted growth of Pb nanoparticles has not previously been reported to the best of our knowledge. The finding that irradiation by X-rays can lead to the formation of a monodisperse population of relatively large nanoparticles of Pb is a rather unexpected result. Our in-situ SAXS measurements show that the growth of these particles is diffusion limited. We have demonstrated that there is no macroscopic heating of our samples by the beam, but note that the time averaged photon power may be misleading when considering local transient effects arising from photon absorption. The small percentage of lead involved in this process suggests that either transient radiation induced defects or trace elements are involved in the process.

The X-ray irradiation did not preclude the growth of nanoparticles of PbS in the irradiated area. A high temperature anneal period in combination with irradiation has thus produced samples containing two distinct populations of nanoparticles. It is interesting to speculate that this phenomenon could be adapted to create functional materials.

Acknowledgements

The Netherlands Organisation for Scientific Research (NWO) and the Swiss Norwegian beamlines are gratefully acknowledged for allowing access to their facilities at the ESRF. We thank Irina Snigireva, ESRF, for the scanning electron microscopy measurements. Eric Schaible is thanked for help with the experiments at the Advanced Light Source. Beamline 7.3.3 of the Advanced Light Source is supported by the Director of the Office of Science, Office of Basic Energy Sciences, of the U.S. Department of Energy under Contract No. DE-AC02-05CH11231. Transmission electron microscopy experiments were performed at NCEM, which is supported by the Office of Science, Office of Basic Energy Sciences of the U.S. Department of Energy under Contract No.: DE-AC02-05CH11231. Other colleagues at the ESRF, particularly Michael Wulff and Mark Newton, are thanked for their helpful discussions.

Notes and references

[a] *Netherlands Organisation for Scientific Research (NWO), DUBBLE@ESRF, 6 Rue Jules Horowitz, 38000 Grenoble, France*
[b] *National Center for Electron Microscopy, Lawrence Berkeley National Laboratory, One Cyclotron Road, MS 72-150, Berkeley, CA 94720-8250, U.S.A.*
[c] *SNBL@ESRF, 6 Rue Jules Horowitz, 38000 Grenoble, France*
[d] *Department of Chemical Engineering and Materials Science, University of California Davis, Davis, California, U.S.A.*
[e] *Materials Technology Group, Department of Mechanical Engineering, Eindhoven University of Technology, Eindhoven, The Netherlands*

†Electronic Supplementary Information (ESI) available: *[SEM image of annealed sample and EXAFS characterization]*

1. R. J. Davies, M. Burghammer and C. Riekel, *Macromolecules*, 2008, **41**, 7251-7253.
2. H. D. Barth, E. A. Zimmermann, E. Schaible, S. Y. Tang, T. Alliston and R. O. Ritchie, *Biomaterials*, 2011, **32**, 8892-8904.
3. J. M. Holton, *Journal Of Synchrotron Radiation*, 2009, **16**, 133-142.
4. V. Martis, S. Nikitenko, S. Sen, G. Sankar, W. van Beek, Y. Filinchuk, I. Snigireva and W. Bras, *Crystal Growth & Design*, 2011, **11**, 2858-2865.
5. D. Tatchev, A. Hoell, M. Eichelbaum and K. Rademann, *Physical Review Letters*, 2011, **106**.
6. P. Innocenzi, L. Malfatti, T. Kidchob, S. Costacurta, P. Falcaro, B. Marmiroli, F. Cacho-Nerin and H. Amenitsch, *Journal of Synchrotron Radiation*, 2011, **18**, 280-286.
7. A. Pinna, B. Lasio, M. Piccinini, B. Marmiroli, H. Amenitsch, P. Falcaro, Y. Tokudome, L. Malfatti and P. Innocenzi, *ACS Applied Materials & Interfaces*, 2013, **5**, 3168-3175.
8. J. G. Mesu, A. M. Beale, F. M. F. de Groot and B. M. Weckhuysen, *Journal of Physical Chemistry B*, 2006, **110**, 17671-17677.
9. R. A. Mayanovic, A. J. Anderson, H. A. N. Dharmagunawardhane, S. Pascarelli and G. Aquilanti, *Journal Of Synchrotron Radiation*, 2012, **19**, 797-805.
10. V. I. Feldman, A. A. Zezin, S. S. Abramchuk and E. A. Zezina, *Journal of Physical Chemistry C*, 2013, **117**, 7286-7293.
11. A. Merlino, M. R. Fuchs, A. Pica, A. Balsamo, F. S. N. Dworkowski, G. Pompidor, L. Mazzarella and A. Vergara, *Acta Crystallographica Section D-Biological Crystallography*, 2013, **69**, 137-140.
12. G. N. George, I. J. Pickering, M. J. Pushie, K. Nienaber, M. J. Hackett, I. Ascone, B. Hedman, K. O. Hodgson, J. B. Aitken, A. Levina, C. Glover and P. A. Lay, *Journal of Synchrotron Radiation*, 2012, **19**, 875-886.
13. E. F. Garman and R. L. Owen, *Acta Crystallographica Section D-Biological Crystallography*, 2006, **62**, 32-47.
14. E. F. Garman, *Acta Crystallographica Section D-Biological Crystallography*, 2010, **66**, 339-351.
15. H. Jain, *Journal of Optoelectronics and Advanced Materials*, 2003, **5**, 5-22.
16. A. Mhaisekar, M. J. Kazmierczak and R. Banerjee, *Journal of Synchrotron Radiation*, 2005, **12**, 318-328.
17. S. D. Stookey, G. H. Beall and J. E. Pierson, *Journal of Applied Physics*, 1978, **49**, 5114-5123.
18. B. Capoen, A. Chahadih, H. El Hamzaoui, O. Cristini and M. Bouazaoui, *Nanoscale Research Letters*, 2013, **8**.
19. G. Mattei, P. Mazzoldi and H. Bernas, *Materials Science with Ion Beams*, 2010, **116**, 287-316.
20. J. Li, X. Y. Hu, Y. Gu and Q. H. Gong, *Optics Letters*, 2010, **35**, 4051-4053.
21. Y. Tang and W. L. Cheng, *Langmuir*, 2013, **29**, 3125-3132.
22. G. Li and R. C. Jin, *Accounts of Chemical Research*, 2013, **46**, 1749-1758.
23. S. V. Kershaw, A. S. Susha and A. L. Rogach, *Chemical Society Reviews*, 2013, **42**, 3033-3087.
24. F. W. Wise, *Accounts of Chemical Research*, 2000, **33**, 773-780.
25. G. Kellermann and A. F. Craievich, *Physical Review B*, 2004, **70**, 054106.
26. J. A. Jimenez, M. Sendova and H. Liu, *Journal of Luminescence*, 2011, **131**, 535-538.
27. W. Bras, G. N. Greaves, M. Oversluizen, S. M. Clark and G. Eeckhaut, *Journal of Non-Crystalline Solids*, 2005, **351**, 2178-2193.
28. W. Bras, S M Clark, G N Greaves, M Kunz, W van Beek and V. Radmilovic, *Crystal Growth Design*, 2009, **9**, 1297.
29. L. Malfatti, D. Marongiu, S. Costacurta, P. Falcaro, H. Amenitsch, B. Marmiroli, G. Grenci, M. F. Casula and P. Innocenzi, *Chemistry of Materials*, 2010, **22**, 2132-2137.
30. S. Nikitenko, A. M. Beale, A. M. J. van der Eerden, S. D. M. Jacques, O. Leynaud, M. G. O'Brien, D. Detollenaere, R. Kaptein, B. M. Weckhuysen and W. Bras, *Journal Of Synchrotron Radiation*, 2008, **15**, 632-640.

31. W. Bras, I. P. Dolbnya, D. Detollenaere, R. van Tol, M. Malfois, G. N. Greaves, A. J. Ryan and E. Heeley, *Journal of Applied Crystallography*, 2003, **36**, 791-794.
32. P. Alexander Hexemer and Wim Bras and James Glossinger and Eric Schaible and Eliot Gann and Rick Kirian and Alastair MacDowell and Matthew Church and Bruce Rude and Howard, *Journal of Physics: Conference Series*, 2010, **247**, 012007.
33. C. Broennimann, E. F. Eikenberry, B. Henrich, R. Horisberger, G. Huelsen, E. Pohl, B. Schmitt, C. Schulze-Briese, M. Suzuki, T. Tomizaki, H. Toyokawa and A. Wagner, *J Synchrotron Radiat*, 2006, **13**, 120-130.
34. A. P. Hammersley, S. O. Svensson, M. Hanfland, A. N. Fitch and D. Hausermann, *High Pressure Research*, 1996, **14**, 235-248.
35. J. Kohlbrecher, pp. Paul Scherrer Institute, Laboratory for Neutron Scattering, CH-5232 Viligen PSI, Switzerland.
36. C. Broennimann, Dectris Ltd., https://www.dectris.com.
37. M. H. F. Overwijk, F. C. van den Heuvel and C. W. T. Bulle-Lieuwma, *J. Vac. Sci. Technol.*, 1993, **11**, 2021.
38. A. Cumming, P. Wiltzius and F. S. Bates, *Phys. Rev. Lett.*, 1990, **65**, 863--866.
39. S. Maruno and T. Kawaguchi, *Journal of Applied Physics*, 1975, **46**, 5312-5314.
40. N. Yoshida and K. Tanaka, *Journal of Applied Physics*, 1995, **78**, 1745-1750.
41. J. W. Sheng, K. Kadono and T. Yazawa, *Journal of Non-Crystalline Solids*, 2003, **324**, 295-299.
42. S. Reibstein, D. Möncke, J. Herbst, D. Schumacher, A. Höll and L. Wondraczek, presented in part at the 12th International Conference on the Structure of Non-crystalline Materials (NCM12), Riva del Garda, Italy, 2013.
43. M. Eichelbaum, K. Rademann, A. Hoell, D. M. Tatchev, W. Weigel, R. Stosser and G. Pacchioni, *Nanotechnology*, 2008, **19**.
44. P. G. Ferreira, D. de Ligny, O. Lazzari, A. Jean, O. C. Gonzalez and D. R. Neuville, *Chemical Geology*, 2013, **346**, 106-112.
45. J. Zhang and J. Sheng, *Optical Materials*, 2013, **35**, 1138-1140.
46. S. Vahedi, G. Okada, B. Morrell, E. Muzar, C. Koughia, A. Edgar, C. Varoy, G. Belev, T. Wysokinski, D. Chapman and S. Kasap, *Journal of Applied Physics*, 2012, **112**.
47. A. Corrias, personal communication.
48. I. A. Shkrob, B. M. Tadjikov and A. D. Trifunac, *Journal of Non-Crystalline Solids*, 2000, **262**, 6-34.
49. I. A. Shkrob and V. F. Tarasov, *Journal of Chemical Physics*, 2000, **113**, 10723-10732.
50. D. S. Whittaker, E. Wagenaars and G. J. Tallents, *Physics of Plasmas*, 2011, **18**.
51. D. S. Whittaker, E. Wagenaars and G. J. Tallents, *Physics of Plasmas*, 2011, **18**, 7.
52. Fitch, *International Tables for Crystallography*.
53. T. Xie, L. L. Bai, J. Y. Liu, G. Q. Zhao, X. H. Sun and J. Zhong, *Carbon*, 2013, **56**, 385-388.
54. C. X. Zhao, Y. F. Li, Y. C. Chen, J. Q. Wu, B. Wang, F. T. Yi, S. Z. Deng, N. S. Xu and J. Chen, *Nanotechnology*, 2013, **24**.
55. J. H. Hubbell and S. M. Seltzer, NIST: X-Ray Mass Attenuation Coefficients, http://www.nist.gov/pml/data/xraycoef/.
56. W. E. Schiesser, *The numerical method of lines : integration of partial differential equations*, Academic Press ;, London,, 1991.
57. G. I. and S. J., *The vitreous state, Thermodynamics,Structure, Rheology and Crystallization*, Springer, Berlin, 1995.
58. V. M. Fokin, E. D. Zanotto, N. S. Yuritsyn and J. W. P. Schmelzer, *Journal of Non-Crystalline Solids*, 2006, **352**, 2681–2714.

Figure 1 Evolution of the SAXS patterns over an in-situ 5 hour anneal at 640°C. Curves are shown for 30 minute intervals and are displaced vertically for clarity. The presence of several fringes is characteristic of a very monodisperse distribution

Figure 2 Representative SAXS data from sample annealed for 2hrs 40 minutes at 640°C. The data are fitted by a bimodal distribution of solid spheres. The inset shows the particle size distribution obtained with this fit

Figure 3 The fitted particle radius (Pb particles) as function of time illustrating the initial $R \sim \sqrt{t}$ behaviour indicating a diffusion limited growth process, and the crossover to (tentatively) Ostwald ripening

Figure 4 Powder diffraction data (BM01, ESRF) of an annealed glass sample exposed to X-rays whilst at elevated temperatures after background subtraction. Below the data the solid blue line is the contribution from PbS and the red line with narrower peaks highlights a metallic lead phase. Other peaks are associated with unidentified crystallites

Figure 5 The difference between XRD patterns taken in an irradiated and non-irradiated area of the same sample. Solid line (Pb calculated) is a fit to the crystal structure of lead with lattice parameter 4.9506Å (fixed) and Lorentzian peak broadening

Figure 6 STEM image of region of sample irradiated in-situ at 640 °C for 5 hours in the SAXS experiment revealing a large number of small PbS particles and a small number of larger Pb particles. The sample is thinned to two different thicknesses.

Figure 7 Particle size histogram computed from the circular Hough transform of (total number) particles from the STEM image. There are a large number of small particles and a few much larger particles.

Figure 8 STEM image of region of sample *adjacent* to an area irradiated in-situ at 640 °C for 5 hours in the SAXS experiment. There are no large Pb particles.

Figure 9 transient heating calculated for a nanoparticle of lead embedded in a borosilicate glass matrix

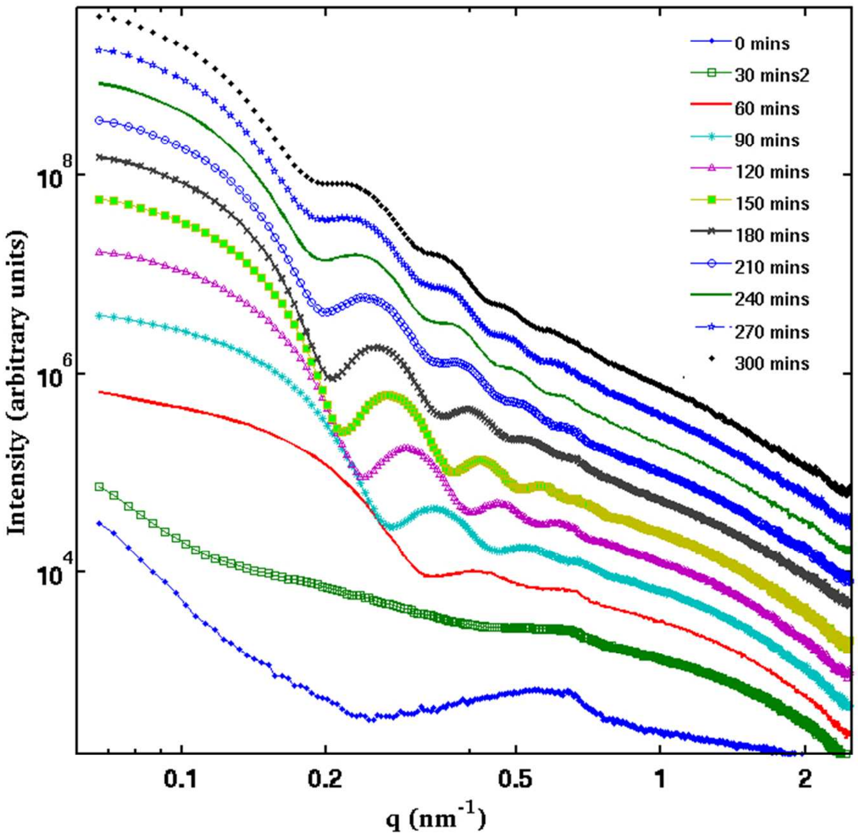

Figure 1 Evolution of the SAXS patterns over an in-situ 5 hour anneal at 640°C. Curves are shown for 30 minute intervals and are displaced vertically for clarity. The presence of several fringes is characteristic of a very monodisperse distribution
277x253mm (75 x 75 DPI)

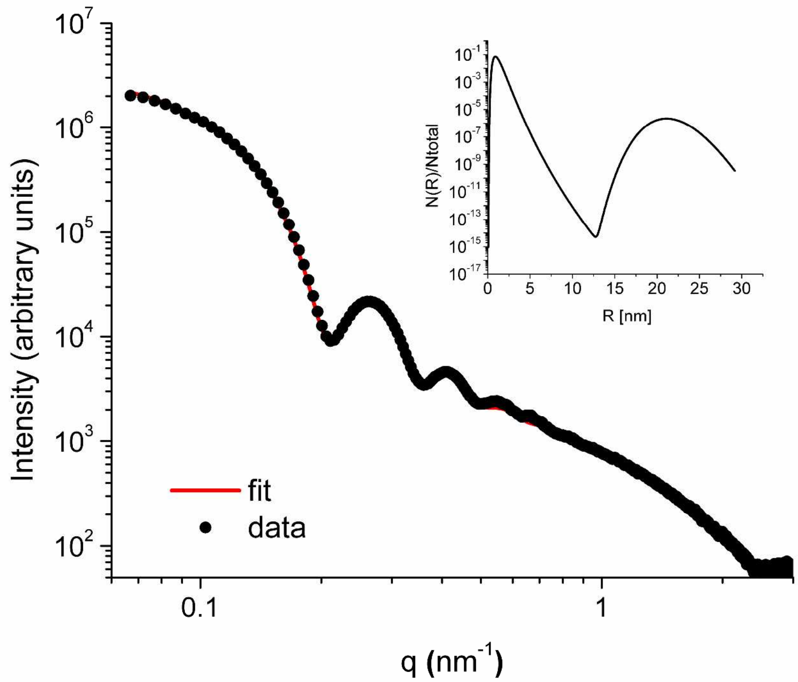

Figure 2 Representative SAXS data from sample annealed for 2hrs 40 minutes at 640℃. The data are fitted by a bimodal distribution of solid spheres. The inset shows the particle size distribution obtained with this fit
1117x863mm (150 x 150 DPI)

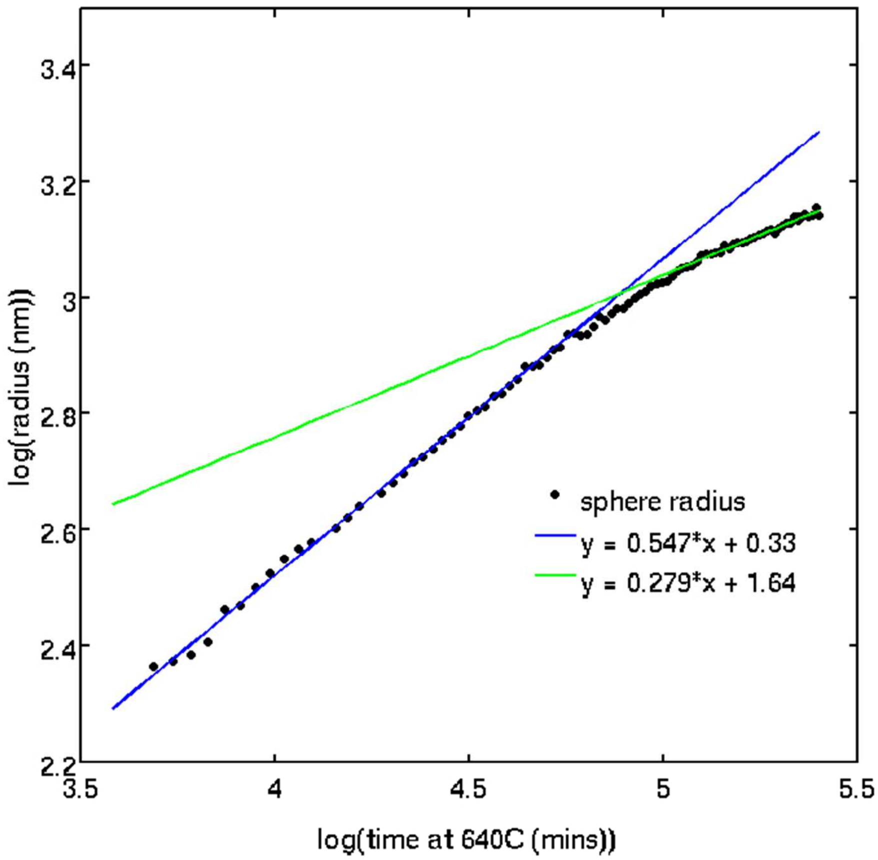

Figure 3 The fitted particle radius (Pb particles) as function of time illustrating the initial R~√t behaviour indicating a diffusion limited growth process, and the crossover to (tentatively) Ostwald ripening
261x242mm (75 x 75 DPI)

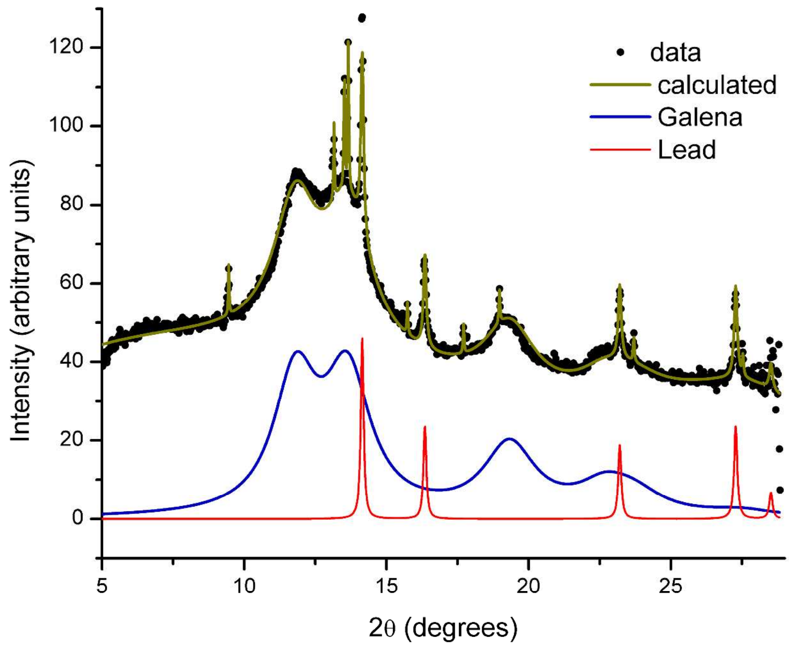

Figure 4 Powder diffraction data (BM01, ESRF) of an annealed glass sample exposed to X-rays whilst at elevated temperatures after background subtraction. Below the data the solid blue line is the contribution from PbS and the red line with narrower peaks highlights a metallic lead phase. Other peaks are associated with unidentified crystallites
800x612mm (150 x 150 DPI)

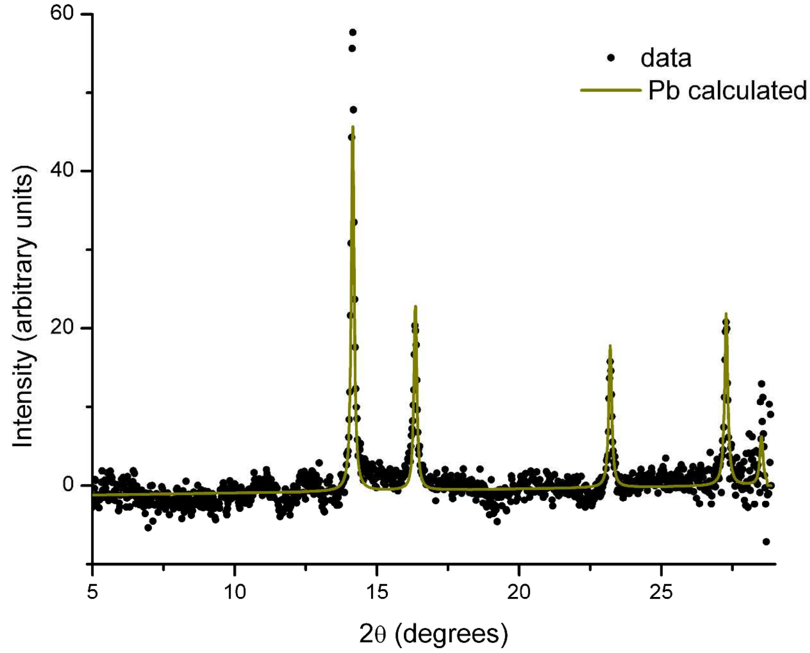

Figure 5 The difference between XRD patterns taken in an irradiated and non-irradiated area of the same sample. Solid line (Pb calculated) is a fit to the crystal structure of lead with lattice parameter 4.9506Å (fixed) and Lorentzian peak broadening
800x612mm (150 x 150 DPI)

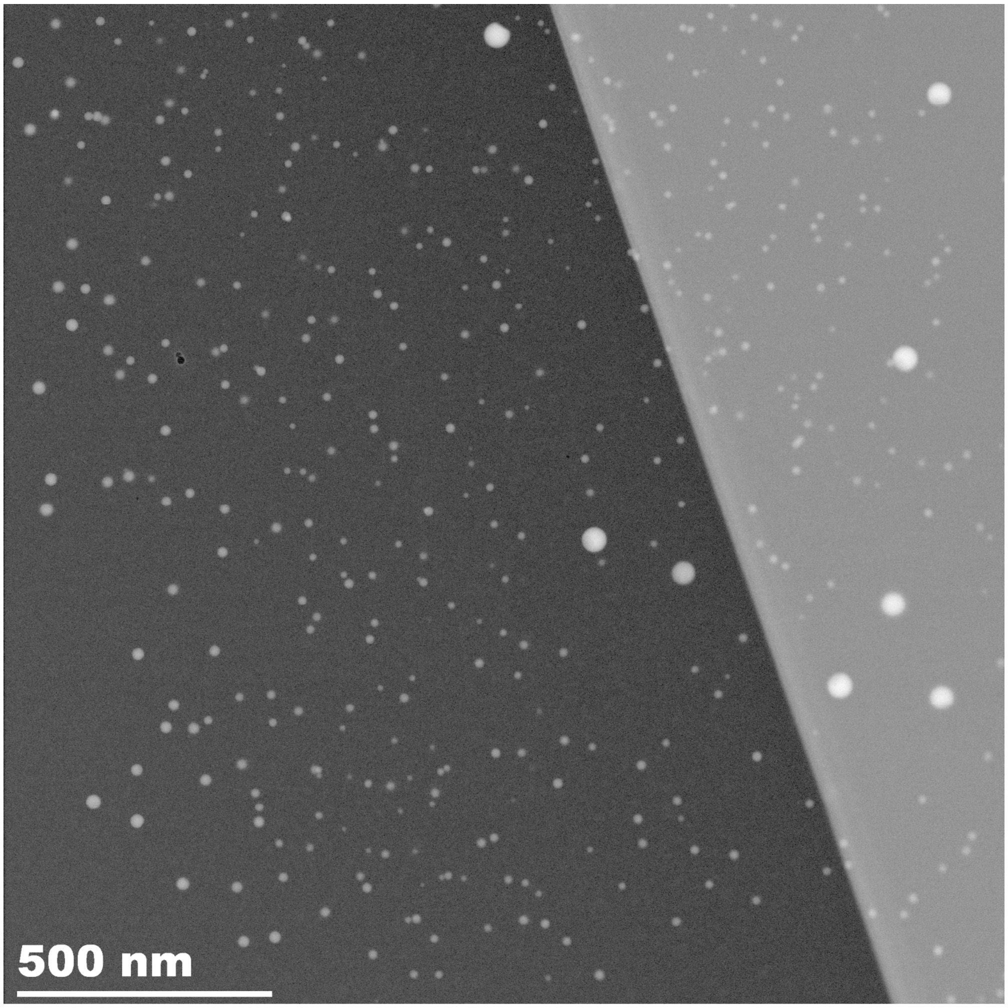

Figure 6 STEM image of region of sample irradiated in-situ at 640 °C for 5 hours in the SAXS experiment revealing a large number of small PbS particles and a small number of larger Pb particles. The sample is thinned to two different thicknesses.

722x722mm (72 x 72 DPI)

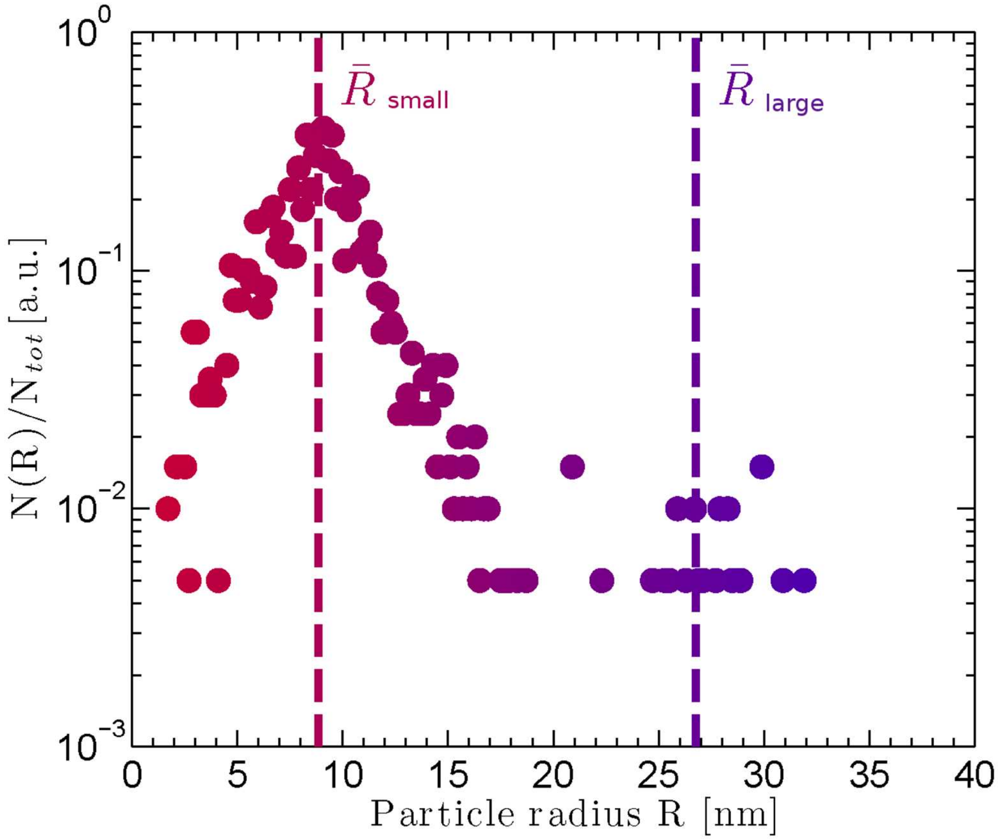

Figure 7 Particle size histogram computed from the circular Hough transform of (total number) particles from the STEM image. There are a large number of small particles and a few much larger particles.
169x143mm (200 x 200 DPI)

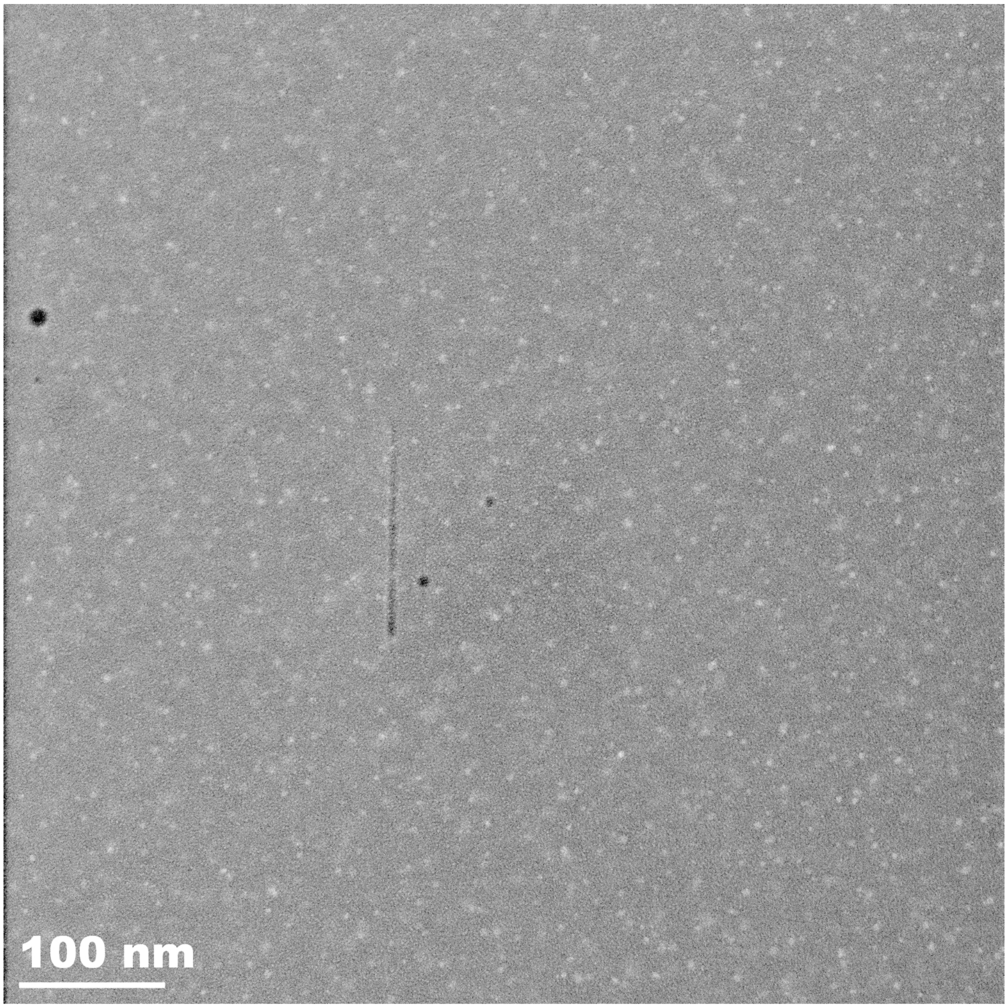

Figure 8 STEM image of region of sample adjacent to an area irradiated in-situ at 640 $^{\circ}$C for 5 hours in the SAXS experiment. There are no large Pb particles.
722x722mm (72 x 72 DPI)

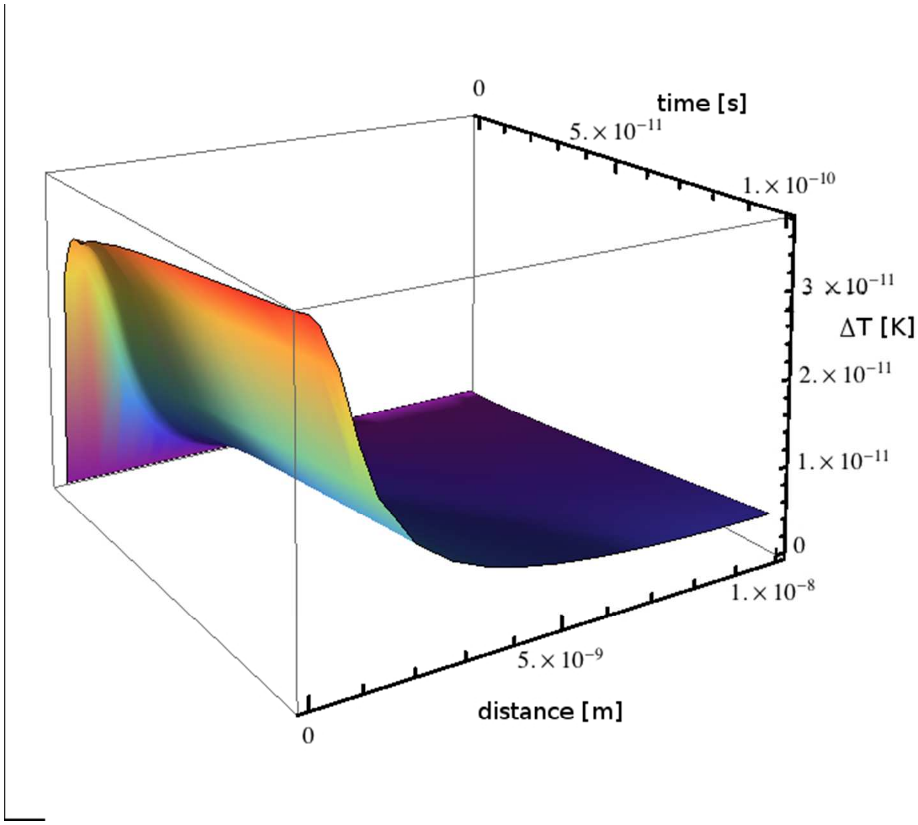

Figure 9 transient heating calculated for a nanoparticle of lead embedded in a borosilicate glass matrix
264x215mm (72 x 72 DPI)